Construction of the crystal potential from the quasi-ion approach

C. Falter, H. Rakel, M. Klenner, and W. Ludwig
Institut für Theoretische Physik II der Westfälischen Wilhelms-Universität Münster, Wilhelm-Klemm-Strasse 10, D-4400 Münster, West Germany
(Received 25 April 1989)

A method for the construction of the crystal potential within the quasi-ion approach is presented and its relation to the Kohn-Sham effective potential is shown. It is demonstrated for Si how this procedure can be used to calculate both the electronic band structure and the phonon dispersion within a simple model for the quasi-ion. Further, the representation of the exchange-correlation-potential and the band-structure potential is discussed, with nonlocality effects taken into account.

I. INTRODUCTION

Calculations of the electronic band structure of semiconductors have had a long history. In earlier work the (local) empirical pseudopotential method[1,2] as well as its nonlocal extension[3] have been used to calculate successfully the band structures and pseudocharge densities of diamond- and zinc-blende-structure semiconductors. In these calculations a few Fourier components (form factors) of the empirical pseudopotential are used and regarded as adjustable parameters. In more recent work, model potentials for the bare ions, rather than the screened pseudopotential (or form factors), have been introduced, which were self-consistently screened with the valence charge.[4–6] In the case of Si it was found[6] that "soft-core" as well as "hard-core" pseudopotentials lead to energy bands which agree in general with each other. The soft-core charge density gives a slightly more distorted bond-charge shape. The minimal band gap in Si, however, is 50% that of germanium, even 100% too small.[7] One of the major problems in these calculations of band structures in solids is the treatment of the electron-electron interaction. The approach to the exchange-correlation part of the potential is provided by Hohenberg-Kohn density-functional theory[8,9] (DFT) and in particular by the Kohn-Sham local-density approximation (LDA). The single-particle eigenvalues of the effective one-electron Schrödinger equation as derived by Kohn and Sham are used to construct the band structures and there is often a fairly good agreement. However, it has been shown that even the exact DFT band structure suffers from the low-band-gap problem (see, e.g., Refs. 10 and 11). In a strict many-body theory the band-structure energies are the energies of the quasiparticles which have to be calculated from a Schrödinger-type equation where the exchange-correlation potential of the Kohn-Sham equation has to be replaced by the self-energy which is a nonlocal energy-dependent operator. Calculations within this formalism are very complex. Using certain approximations for the self-energy (Hedin *GW* approximation[12]) such calculations have recently been performed in semiconductors[13,14,16,17] and corrections to the DFT band structures have been found.

In the present paper we discuss a method which allows for both the calculation of the electronic band structure and the phonon dispersion by a definite model within the quasi-ion approach recently proposed.[18–21] In Sec. II the quasi-ion method is briefly reviewed and the construction of the crystal potential is described. The resulting expression is related to the effective potential of the Kohn-Sham equation. The subject of Sec. III is the development of a pragmatic model to approximate the exchange-correlation contribution to the band-structure potential established in Sec. II. Finally Sec. IV gives the results for the electronic band structure and the phonon dispersion of Si using a simple model for the quasi-ions. The corresponding charge density, crystal potential, and the exchange-correlation contribution are explicitly displayed and discussed in real space.

II. CONSTRUCTION OF THE CRYSTAL POTENTIAL

In the quasi-ion method,[18–21] it is assumed that the electrons follow the motion of the ions adiabatically (Born-Oppenheimer approximation).[22] This means that the electrons realize that the nuclei are at rest in their instantaneous positions and the ions feel the electrons as charge clouds without internal dynamics. Such a picture had led in the past to some attempts to describe the electronic subsystem in a base for the wave functions which follows the motion of the ions instantaneously.[23–25] Mathematically this is achieved by unitary-transformation techniques which preserve orthonormality. However, there is no unique prescription how to construct the moving base.

Within the quasi-ion approach the electronic density $\rho(\mathbf{r})$ instead of the wave functions is taken as the basic variable of the system and it is shown that the latter can be decomposed uniquely into partial densities $\rho^{\mathbf{A}}(\mathbf{r})$ or $\rho_\alpha(\mathbf{r})$ which are assigned to the single ions $\mathbf{A}$ or ion types (sublattices) α, respectively. $\rho^{\mathbf{A}}(\mathbf{r})$ together with the corresponding ion core located at $\mathbf{R}^{\mathbf{A}}=\mathbf{R}^{\mathbf{a}}+\mathbf{R}^{\alpha}$ ($\mathbf{a}$, α cell, and nonprimitive basis index of the crystal) define the quasi-ion. These objects can be interpreted as the new composite building blocks ("dressed ions") of the struc-

ture. They describe that part of the displacement-induced charge-density variation that rigidly follows the motion of the ions. The remaining part is due to distortions during that motion.[21,26,27] The partial densities are defined by investigating the response of the system when the ions are displaced. Formally this is done by calculating the changes in the density induced by moving the ions in a long-wavelength acoustic-phonon mode. As described in Ref. 19 this means to use the acoustic sum rule for determining the charge density. This leads to the result represented in Fourier space;

$$\rho(\mathbf{q}+\mathbf{G})=\sum_{\alpha}\rho_{\alpha}(\mathbf{q}+\mathbf{G})\rightarrow\rho(\mathbf{G})=\sum_{\alpha}\rho_{\alpha}(\mathbf{G}) \quad \text{as } \mathbf{q}\rightarrow\mathbf{0} , \tag{1}$$

with the partial density

$$\rho_{\alpha}(\mathbf{q}+\mathbf{G})=\frac{1}{4\pi}\sum_{j}[v_{|j}(\mathbf{q}+\mathbf{G})]^{*}P^{\alpha}_{|j}(\mathbf{q}+\mathbf{G}) , \tag{2}$$

$$P^{\alpha}_{|j}(\mathbf{q}+\mathbf{G})=\sum_{\mathbf{G}'}D(\mathbf{q}+\mathbf{G},\mathbf{q}+\mathbf{G}')V^{\alpha}_{|j}(\mathbf{q}+\mathbf{G}') , \tag{3}$$

$$V^{\alpha}_{|j}(\mathbf{q}+\mathbf{G})=-i(\mathbf{q}+\mathbf{G})_{j}V_{\alpha}(\mathbf{q}+\mathbf{G})e^{-i\mathbf{G}\cdot\mathbf{R}^{\alpha}} ,$$
$$v_{|j}(\mathbf{q})=-iq_{j}\frac{4\pi}{q^{2}} . \tag{4}$$

$\mathbf{q}$ is a vector from the first Brillouin zone and $\mathbf{G}$ is a reciprocal-lattice vector. D means the static density-response function (matrix) and V_{α} is the ionic (pseudo)potential corresponding to an ion of sublattice α. The quasi-ions can also be represented in direct space:

$$\rho(\mathbf{r})=\sum_{\mathbf{A}}\rho^{\mathbf{A}}(\mathbf{r})=\sum_{\mathbf{A}}\rho_{\alpha}(\mathbf{r}-\mathbf{A}) , \tag{5}$$

with

$$\rho^{\mathbf{A}}(\mathbf{r})=\frac{1}{4\pi}\int dV'\int dV''\sum_{j}v_{|j}(\mathbf{r}-\mathbf{r}')D(\mathbf{r}',\mathbf{r}'')\frac{\partial}{\partial A_{j}}\times V_{\alpha}(\mathbf{r}''-\mathbf{A}) , \tag{6}$$

$$v_{|j}(\mathbf{r}-\mathbf{r}')=\frac{\partial}{\partial r_{j}}|\mathbf{r}-\mathbf{r}'|^{-1} , \tag{7}$$

or

$$\rho^{\mathbf{A}}(\mathbf{r})=\frac{1}{4\pi}\int dV'\,\nabla v(\mathbf{r}-\mathbf{r}')\cdot\mathbf{P}^{\mathbf{A}}(\mathbf{r}') . \tag{8}$$

Here the vector field $\mathbf{P}^{\mathbf{A}}(\mathbf{r})$ with components

$$P^{\mathbf{A}}_{|j}(\mathbf{r})=\int dV'\,D(\mathbf{r},\mathbf{r}')\frac{\partial}{\partial A_{j}}V_{\alpha}(\mathbf{r}'-\mathbf{A}) \tag{9}$$

has been introduced. This field describes the charge-density variation at the space point $\mathbf{r}$ in response to a unit displacement of ion $\mathbf{A}$ in direction j. It can be decomposed into a gradient and a rotational part

$$\mathbf{P}^{\mathbf{A}}(\mathbf{r})=-\nabla\rho^{\mathbf{A}}(\mathbf{r})+\nabla\times\mathbf{W}^{\mathbf{A}}(\mathbf{r}) . \tag{10}$$

The quasi-ion contribution represents the rigid part of the density variation while the distortions are given by the curl of the field $\mathbf{W}^{\mathbf{A}}(\mathbf{r})$.

The partial densities are strongly localized objects in direct space. This has been shown in Refs. 18, 20, and 27 and can also be understood on physical grounds. If the crystal is perturbed by a displacement of the ionic potential the change in energy is minimized by a rearrangement of the electronic charge. This results in a screening of the change in the ionic potential and thus to a tendency to maintain local charge neutrality. In direct space this mechanism leads to localized objects which consist of the bare ion plus a fairly well localized distribution of electronic charge which is constrained by the local geometry of the surrounding structure.

Thus an expansion of $\rho_{\alpha}(\mathbf{r})$ into a small set of localized *ansatz* functions, e.g., spherical Gaussians, is appropriate,

$$\rho_{\alpha}(\mathbf{r})=\sum_{\mu}\left[\frac{\gamma^{\alpha}_{\mu}}{\pi}\right]^{3/2}C^{\alpha}_{\mu}\exp[-\gamma^{\alpha}_{\mu}(\mathbf{r}-\mathbf{R}^{\alpha}_{\mu})^{2}] . \tag{11}$$

C^{α}_{μ}, γ^{α}_{μ}, and $\mathbf{R}^{\alpha}_{\mu}$ denote the amplitude, decay constant, and localization center of the μth *ansatz* Gaussian of ion type α, respectively.

In Fig. 1 we have reproduced the contour plot of $\rho_{\alpha}(\mathbf{r})$ in Si as obtained within the simple model discussed in Ref. 18. A set of three Gaussians centered at an ion and another three Gaussians centered at each of the four bonds has been used only. We shall take this model for ρ_{α} in Sec. IV without any changes for an approximate description of the crystal potential and the band structure.

The construction of the crystal potential $V_{\text{eff}}(\mathbf{r})$ in terms of the partial densities follows in an analogous way as the charge density from its variation when a long-wavelength acoustic phonon is impressed on the crystal. The results are similar to those for the density if the density-response function is replaced by the inverse of the dielectric function. Thus we obtain

$$V_{\text{eff}}(\mathbf{r})\equiv\sum_{\mathbf{G}}\tilde{V}(\mathbf{G})e^{i\mathbf{G}\cdot\mathbf{r}} , \tag{12}$$

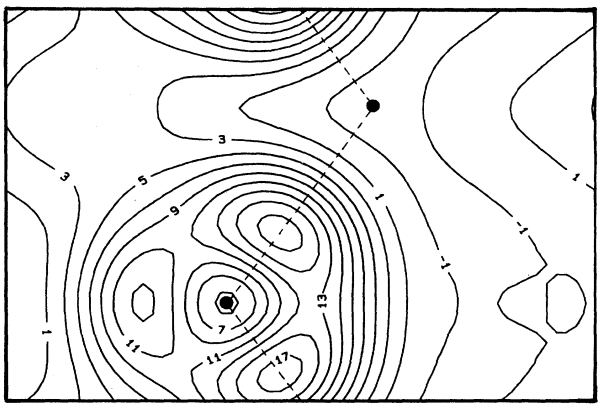

FIG. 1. Contour plot of the partial density $\rho_{\alpha}(\mathbf{r})$ of Si in the $(0,-1,1)$ plane as calculated from Eq. (11). Units in electrons per cell. The bonds in the plane are indicated by dashed lines and the ions are indicated by dots.

with

$$\tilde{V}(\mathbf{G})=\frac{1}{V_z}\lim_{\mathbf{q}\to 0}\left\{\sum_\alpha\left[\frac{1}{4\pi}\sum_j[v_{|j}(\mathbf{q}+\mathbf{G})]^*\times\sum_{\mathbf{G}'}\epsilon^{-1}(\mathbf{q}+\mathbf{G},\mathbf{q}+\mathbf{G}')\times V^\alpha_{|j}(\mathbf{q}+\mathbf{G}')\right]\right\} \quad (13)$$

(with V_z the volume of an elementary cell).

Using the relation between the inverse dielectric function (matrix) ϵ^{-1} and the density-response function (matrix)[21]

$$\epsilon^{-1}=1+\tilde{v}D,\quad D=\pi\epsilon^{-1}=\pi(1-\tilde{v}\pi)^{-1}\ , \quad (14)$$

where

$$\tilde{v}=v-v_{\mathrm{xc}}\ , \quad (15)$$

denotes the effective electron-electron interaction which consists of the Coulomb interaction v and the exchange-correlation contribution

$$v_{\mathrm{xc}}(\mathbf{r},\mathbf{r}')=-\frac{\delta^2E_{\mathrm{xc}}[\rho]}{\delta\rho(\mathbf{r})\,\delta\rho(\mathbf{r}')} \quad (16)$$

($E_{\mathrm{xc}}[\rho]$ exchange-correlation functional of density-functional theory), we can express Eq. (13) in the following form:

$$\tilde{V}(\mathbf{G})=\frac{1}{V_z}\lim_{\mathbf{q}\to 0}\left\{\sum_\alpha\left[\frac{1}{4\pi}\sum_j[v_{|j}(\mathbf{q}+\mathbf{G})]^*\left[V^\alpha_{|j}(\mathbf{q}+\mathbf{G})+v(\mathbf{q}+\mathbf{G})P^\alpha_{|j}(\mathbf{q}+\mathbf{G})-\sum_{\mathbf{G}''}v_{\mathrm{xc}}(\mathbf{q}+\mathbf{G},\mathbf{q}+\mathbf{G}'')P^\alpha_{|j}(\mathbf{q}+\mathbf{G}'')\right]\right]\right\}. \quad (17)$$

Here the Fourier transform of the vector field $\mathbf{P}^{\mathbf{A}}$ from Eq. (9) has been introduced, i.e.,

$$P^\alpha_{|j}(\mathbf{q}+\mathbf{G})=\sum_{\mathbf{G}'}D(\mathbf{q}+\mathbf{G},\mathbf{q}+\mathbf{G}')V^\alpha_{|j}(\mathbf{q}+\mathbf{G}')\ . \quad (18)$$

Equation (17) relates the crystal potential (band-structure potential) to the vector field $\mathbf{P}^{\mathbf{A}}(\mathbf{r})$ and thus to the density response of the system. Thus it becomes possible to investigate the electronic band structure, lattice dynamics, and the electron-phonon interaction within a certain model for the quasi-ion. Concerning the exchange-correlation contribution the same expression v_{xc} appears in the calculation for both the crystal potential and the density-response function. Physically v_{xc} means an exchange-correlation interaction that describes the change of the exchange-correlation potential V_{xc},

$$V_{\mathrm{xc}}(\mathbf{r})=\frac{\delta E_{\mathrm{xc}}[\rho]}{\delta\rho(\mathbf{r})}\ ,\qquad \delta V_{\mathrm{xc}}(\mathbf{r})=\int dV'\frac{\delta^2E_{\mathrm{xc}}[\rho]}{\delta\rho(\mathbf{r})\,\delta\rho(\mathbf{r}')}\delta\rho(\mathbf{r}')\ , \quad (19)$$

which is induced by the variation of the external potential. In the simple model of Sec. III, v_{xc} will be approximated in form of a static local-field factor which is used in the theory of the dielectric function[28] to simulate exchange-correlation effects in homogeneous systems. Thus we have found an alternative way to express the Kohn-Sham equation by coupling the induced change of the exchange-correlation (XC) potential to the induced charge-density variation. Furthermore it becomes obvious how nonlocality effects explicitly enter via v_{xc} the calculation of the band structure; see in addition Eqs. (24) and (28). The interrelation with the usual version of the Kohn-Sham equation is discussed below.

Next we introduce a diagonal approximation for v_{xc} in Eq. (17),

$$v_{\mathrm{xc}}(\mathbf{q}+\mathbf{G},\mathbf{q}+\mathbf{G}')\approx v_{\mathrm{xc}}(\mathbf{q}+\mathbf{G})\delta_{\mathbf{G}\mathbf{G}'}\ . \quad (20)$$

The resulting crystal potential then reads as

$$\tilde{V}(\mathbf{G})=\frac{1}{V_z}\lim_{\mathbf{q}\to 0}\sum_\alpha\left[\frac{1}{4\pi}\sum_j[v_{|j}(\mathbf{q}+\mathbf{G})]^*V^\alpha_{|j}(\mathbf{q}+\mathbf{G})+\tilde{v}(\mathbf{q}+\mathbf{G})\frac{1}{4\pi}\sum_j[v_{|j}(\mathbf{q}+\mathbf{G})]^*P^\alpha_{|j}(\mathbf{q}+\mathbf{G})\right]. \quad (21)$$

Following the discussion in Refs. 19 and 21, the nonanalytic terms in $P^\alpha_{|j}(\mathbf{q}+\mathbf{G})$ for $\mathbf{G}\neq\mathbf{0}$ vanish (ASR); we obtain

$$\lim_{\mathbf{q}\to 0}\sum_\alpha\mathbf{P}^\alpha(\mathbf{q}+\mathbf{G})=\sum_\alpha\hat{\mathbf{P}}^\alpha(\mathbf{G}),\quad \mathbf{G}\neq\mathbf{0} \quad (22)$$

where $\hat{\mathbf{P}}^\alpha(\mathbf{G})$ is the analytic part of the vector field. Thus the crystal potential can be written as a superposition of quasi-ion potentials[21]

$$\tilde{V}(\mathbf{G})=\sum_\alpha\tilde{V}_\alpha(\mathbf{G})\ , \quad (23)$$

with

$$\tilde{V}_\alpha(\mathbf{G})=\frac{1}{V_z}\left[\frac{1}{4\pi}\sum_j[v_{|j}(\mathbf{G})]^*V^\alpha_{|j}(\mathbf{G})+\tilde{v}(\mathbf{G})\rho_\alpha(\mathbf{G})\right], \quad (24)$$

$$\rho_\alpha(\mathbf{G})=\frac{1}{4\pi}\sum_j[v_{|j}(\mathbf{G})]^*\hat{P}^\alpha_{|j}(\mathbf{G}),\quad \mathbf{G}\neq\mathbf{0} \quad (25)$$

and

$$\tilde{V}(0)=\frac{1}{V_z}\lim_{\mathbf{q}\to 0}\sum_{\alpha}\left[\frac{1}{4\pi}\sum_{j}[v_{|j}(\mathbf{q})]^{*}V^{\alpha}_{|j}(\mathbf{q})+\tilde{v}(\mathbf{q})\rho_{\alpha}(\mathbf{q})\right], \tag{26}$$

$$\rho_{\alpha}(\mathbf{q})=\frac{1}{4\pi}\sum_{j}[v_{|j}(\mathbf{q})]^{*}P^{\alpha}_{|j}(\mathbf{q}) . \tag{27}$$

It is important to realize that the XC potential occurs in this formulation in the product form, $v_{xc}\rho$ with the density appearing directly as a factor. Thus it seems appealing to approximate v_{xc} by a suitable homogeneous electron-gas expression based on the average density of the corresponding semiconductor. Furthermore, testing of local as well as nonlocal models for v_{xc} becomes possible, see Sec. IV.

In order to compare the above approach to the crystal potential with the Kohn-Sham potential we represent $V_{\text{eff}}(\mathbf{r})$ in direct space,

$$V_{\text{eff}}(\mathbf{r})=\sum_{\mathbf{A}}\tilde{V}^{\mathbf{A}}(\mathbf{r})=\sum_{\mathbf{A}}\frac{1}{4\pi}\int dV'\int dV''\sum_{j}v_{|j}(\mathbf{r}-\mathbf{r}')\epsilon^{-1}(\mathbf{r}',\mathbf{r}'')\times\frac{\partial}{\partial A_j}V_{\alpha}(\mathbf{r}''-\mathbf{A}) . \tag{28}$$

See also Ref. 29 for a decomposition of the total potential into rigid quasi-ion potentials $\tilde{V}^{\mathbf{A}}$. Equation (28) can also be expressed as

$$V_{\text{eff}}(\mathbf{r})=-\frac{1}{4\pi}\int dV'\int dV''\,\nabla v(\mathbf{r}-\mathbf{r}')\epsilon^{-1}(\mathbf{r}',\mathbf{r}'')\times\nabla''V(\mathbf{r}'') , \tag{29}$$

where the external potential

$$V(\mathbf{r})=\sum_{\mathbf{A}}V_{\alpha}(\mathbf{r}-\mathbf{A}) \tag{30}$$

has been used. Using the representation

$$\phi(\mathbf{r})=\frac{1}{4\pi}\int dV'\,\nabla' v(\mathbf{r}-\mathbf{r}')\cdot\nabla'\phi(\mathbf{r}') \tag{31}$$

one can deduce from (29) that $V_{\text{eff}}(\mathbf{r})$ is just the Kohn-Sham potential (up to a constant)

$$V^{\text{KS}}(\mathbf{r})=V(\mathbf{r})+V_H(\mathbf{r})+V_{xc}(\mathbf{r}) , \tag{32}$$

$$V_H(\mathbf{r})=\int dV'\,v(\mathbf{r}-\mathbf{r}')\rho(\mathbf{r}') \tag{33}$$

if the relation

$$\int dV''\,\epsilon^{-1}(\mathbf{r}',\mathbf{r}'')\nabla''V(\mathbf{r}'')=\nabla'V^{\text{KS}}(\mathbf{r}') \tag{34}$$

holds.

We have

$$\nabla V_H(\mathbf{r})=\int dV'\,v(\mathbf{r}-\mathbf{r}')\nabla'\rho(\mathbf{r}') \tag{35}$$

and

$$\nabla V_{xc}(\mathbf{r})=-\int dV'\,v_{xc}(\mathbf{r},\mathbf{r}')\nabla'\rho(\mathbf{r}') . \tag{36}$$

The latter relation is obtained because $E_{xc}[\rho]$ is translationally invariant, resulting in

$$\int dV'\frac{\delta E_{xc}[\rho]}{\delta\rho(\mathbf{r}')}\nabla'\rho(\mathbf{r}')=0 . \tag{37}$$

Functional differentiation with respect to $\rho(\mathbf{r})$ then yields Eq. (36), and thus we have

$$\nabla V^{\text{KS}}(\mathbf{r})=\nabla V(\mathbf{r})+\int dV'\,\bar{v}(\mathbf{r},\mathbf{r}')\nabla'\rho(\mathbf{r}') . \tag{38}$$

On the other hand, the left-hand side of Eq. (34) can be written as

$$\nabla V(\mathbf{r})+\int dV''\,\bar{v}(\mathbf{r},\mathbf{r}'')\int dV'\,D(\mathbf{r}'',\mathbf{r}')\nabla'V(\mathbf{r}') . \tag{39}$$

However, this equation is identical to Eq. (38) if the invariance of the system under rigid translations of the external potential $V(\mathbf{r})$ is used,[21] which leads to

$$\nabla\rho(\mathbf{r})=\int dV'\,D(\mathbf{r},\mathbf{r}')\nabla'V(\mathbf{r}') \tag{40}$$

and completes the proof.

III. A SIMPLE MODEL FOR EXCHANGE CORRELATION

In this section we develop a simple model to approximate the exchange-correlation interaction. The resulting expression for v_{xc} will then be used in Eqs. (23)–(26) for the calculation of the band structure in Si. Starting with the rigorous expression of v_{xc} several approximations will be performed which ultimately can be justified only by applying the model to a realistic problem like the calculation of the electronic properties of an inhomogeneous system like Si. It is our intention to extract from the exact $v_{xc}(\mathbf{r},\mathbf{r}')$ a corresponding homogeneous-limit expression where the dependence on $\mathbf{r}$ and $\mathbf{r}'$ is reduced to the dependence on $|\mathbf{r}-\mathbf{r}'|$ and the dependence on $\rho(\mathbf{r})$ is replaced by that on the average density $\bar{\rho}$. Using such a model for v_{xc} in the formulation of the band-structure potential from Eqs. (23)–(27), the dependence of the exchange-correlation potential V_{xc} on the real density of the system is still taken into account by the partial densities $\rho_{\alpha}(\mathbf{G})$.

The exchange-correlation energy can be represented in terms of the exchange-correlation hole[30] as

$$E_{xc}[\rho]=\tfrac{1}{2}\int dV\int dV'\,\rho(\mathbf{r})v(\mathbf{r}-\mathbf{r}')\rho_{xc}(\mathbf{r},\mathbf{r}') , \tag{41}$$

where ρ_{xc} corresponds to the removal of one electron which is expressed by the XC sum rule

$$\int dV'\,\rho_{xc}(\mathbf{r},\mathbf{r}')=-1 . \tag{42}$$

Equations (41) and (42) allow for an interpretation of E_{xc} as the electrostatic interaction energy between the electron density $\rho(\mathbf{r})$ and the hole. The latter describes the probability that an electron at $\mathbf{r}'$ is pushed away if an electron is present at $\mathbf{r}$, due to exchange and correlation.

The XC hole can further be related to the pair correla-

tion function $g_{[\rho]}(\mathbf{r},\mathbf{r}';\alpha)$ for a given coupling constant α,[30]

$$\rho_{xc}(\mathbf{r},\mathbf{r}')=\rho(\mathbf{r}')\int_0^1 d\alpha[g_{[\rho]}(\mathbf{r},\mathbf{r}';\alpha)-1] \equiv\rho(\mathbf{r}')G_{[\rho]}(\mathbf{r},\mathbf{r}') \ . \tag{43}$$

Because of the long-range nature of the Coulomb interaction the detailed shape of ρ_{xc} in Eq. (41) is not as important as its charge. Thus it is essential to satisfy the XC sum rule (42), i.e., charge conservation.

For our purpose it is useful to rewrite Eq. (41),

$$E_{xc}[\rho]\equiv\tfrac{1}{2}\int dV\int dV'\,\rho(\mathbf{r})f_{xc}(\mathbf{r},\mathbf{r}')\rho(\mathbf{r}') \ . \tag{44}$$

$f_{xc}(\mathbf{r},\mathbf{r}')$ is equivalent to $v(\mathbf{r}-\mathbf{r}')G_{[\rho]}(\mathbf{r},\mathbf{r}')$ and this function seems to be well described by an approximation of the homogeneous electron gas, as proposed in Eq. (53). The reason is that the most important range for $G_{[\rho]}(\mathbf{r},\mathbf{r}')$ corresponds to the situation when $\mathbf{r}$ and $\mathbf{r}'$ are close to each other. In this case the weighting factor, i.e., the Coulomb interaction, dominates the $(\mathbf{r},\mathbf{r}')$ dependence of the product.

Functional differentiation of E_{xc} leads to the expression for $v_{xc}(\mathbf{r},\mathbf{r}')$ from Eq. (16),

$$\frac{\delta^2E_{xc}[\rho]}{\delta\rho(\mathbf{r}_1)\,\delta\rho(\mathbf{r}_2)}=\tfrac{1}{2}[f_{xc}(\mathbf{r}_1,\mathbf{r}_2)+f_{xc}(\mathbf{r}_2,\mathbf{r}_1)]+\tfrac{1}{2}\int dV'\frac{\delta f_{xc}(\mathbf{r}_2,\mathbf{r}')}{\delta\rho(\mathbf{r}_1)}\rho(\mathbf{r}')+\tfrac{1}{2}\int dV'\frac{\delta f_{xc}(\mathbf{r}_1,\mathbf{r}')}{\delta\rho(\mathbf{r}_2)}\rho(\mathbf{r}') +\tfrac{1}{2}\int dV\frac{\delta f_{xc}(\mathbf{r},\mathbf{r}_2)}{\delta\rho(\mathbf{r}_1)}\rho(\mathbf{r})+\tfrac{1}{2}\int dV\frac{\delta f_{xc}(\mathbf{r},\mathbf{r}_1)}{\delta\rho(\mathbf{r}_2)}\rho(\mathbf{r})+\tfrac{1}{2}\int dV\int dV'\,\rho(\mathbf{r})\frac{\delta^2 f_{xc}(\mathbf{r},\mathbf{r}')}{\delta\rho(\mathbf{r}_1)\,\delta\rho(\mathbf{r}_2)}\rho(\mathbf{r}') \ . \tag{45}$$

We replace Eq. (45) by taking a local approximation of f_{xc} on ρ in the integrals and perform the homogeneous limit after all integrations have been carried out. This procedure is applied to the single terms in Eq. (45) in such a way that the dependence on $|\mathbf{r}_1-\mathbf{r}_2|$ of v_{xc} is preserved. We write, for example,

$$\int dV'\frac{\delta f_{xc}(\mathbf{r}_2,\mathbf{r}')}{\delta\rho(\mathbf{r}_1)}\rho(\mathbf{r}')\rightarrow\int dV'\frac{\delta f_{xc}(|\mathbf{r}_2-\mathbf{r}'|,\rho(\mathbf{r}'))}{\delta\rho(\mathbf{r}_1)}\rho(\mathbf{r}')=\frac{\delta f_{xc}(|\mathbf{r}_2-\mathbf{r}_1|,\rho)}{\partial\rho}\rho(\mathbf{r}_1)\rightarrow\bar{\rho}\frac{\partial f_{xc}(|\mathbf{r}_2-\mathbf{r}_1|,\bar{\rho})}{\partial\bar{\rho}} \tag{46}$$

etc. After Fourier transformation we obtain the following result:

$$v_{xc}(q,\bar{\rho})=-\left\{f_{xc}(q,\bar{\rho})+2\bar{\rho}\frac{\partial f_{xc}(q,\bar{\rho})}{\partial\bar{\rho}} +\tfrac{1}{2}\bar{\rho}\frac{\partial^2 f_{xc}(q,\bar{\rho})}{\partial\bar{\rho}^2}\bar{\rho}\right\} . \tag{47}$$

Finally, the local-field factor $G(q,\bar{\rho})$ is defined by

$$v_{xc}(q,\bar{\rho})\equiv v(q)G(q,\bar{\rho}) \ . \tag{48}$$

It should be noted that in our formulation of the exchange-correlation potential V_{xc} according to Eqs. (23)–(27) or (61), one is not forced to use the expression of the definite model from Eq. (47) as an approximation for v_{xc} or the local-field factor $G(q)$, respectively. One could also try other forms for $G(q)$ known from the literature.[28,31] On the other hand, Eq. (47) leads to very good results for the band structure. The essential point is that we are able to express V_{xc} approximately in a form where nonlocality effects are represented by the homogeneous limit of v_{xc} and the real density enters as a direct factor. This is similar to the results given in Ref. 17, where it is shown that the nonlocality of the self-energy is well reproduced by that of the self-energy operator in jellium of the average density of the semiconductor. Our calculations in Sec. IV will demonstrate that when using V_{xc} in the product form emerging from the quasi-ion approach even a local approximation for v_{xc} in the homogeneous limit leads to a very good band structure. This might be expected when looking to the discussions of V_{xc} in the literature.[17,32] The shape of this function looks like the density when scaled in an appropriate way.

In order to obtain an efficient computational scheme, we introduce a parametrization of v_{xc} with two parameters only. The latter are fixed by fulfilling the homogeneous limit of the XC sum rule and by using the short-wavelength limit for $G(q,\bar{\rho})$ which is related to the radial distribution function[33] $g(r,\bar{\rho})$,

$$\lim_{q\rightarrow\infty}G(q,\bar{\rho})=1-g(0,\bar{\rho}) \ . \tag{49}$$

For high electronic densities (small Coulomb coupling parameter $r_s\sim\bar{\rho}^{-1/3}$) the Bohm-Pines random-phase approximation [RPA, $v_{xc}=0$ in Eq. (14)] is known to give reasonable results because the kinetic energy is dominant, while for real electronic densities in metals or semiconductors exchange-correlation corrections become important.[34] The behavior of interacting electrons with parallel spin at small interparticle separation is determined by the exclusion principle. On the other hand, Coulomb repulsion dominates the short-range correlations between electrons of antiparallel spin. The latter effect leads to a decrease of the Hartree-Fock value $g_{HF}(0)=\frac{1}{2}$ to lower values. In our model calculation we use the variational results for $g(0,\bar{\rho})$ as given in Ref. 35, which are in good agreement with Monte Carlo–type calculations.[36]

The XC sum rule can be written in the homogeneous limit as

$$\bar{f}_{xc}(q\rightarrow0,\bar{\rho})=-1/\bar{\rho} \ , \tag{50}$$

where $\bar{f}_{xc}$ is defined by

$$\bar{f}_{xc}(|\mathbf{r}-\mathbf{r}'|)=|\mathbf{r}-\mathbf{r}'|f_{xc}(|\mathbf{r}-\mathbf{r}'|)\ . \tag{51}$$

The ansatz chosen for $f_{xc}(q)$ is

$$f_{xc}(q)=A(1-e^{-\varphi q^2})v(q) \tag{52}$$

or

$$f_{xc}(r)=A\frac{\mathrm{erfc}(\gamma r)}{r},\quad \gamma=\frac{1}{2\sqrt{\varphi}}\ . \tag{53}$$

This leads, for $\bar{f}_{xc}(q)$, to the result

$$\bar{f}_{xc}(q)=A\frac{8\sqrt{\pi}}{q^3}[(1+2\varphi q^2)D(\sqrt{\varphi}q)-\sqrt{\varphi}q] \tag{54}$$

with Dawson's integral[37]

$$D(x)=e^{-x^2}\int_0^x dt\,\exp(t^2)\ . \tag{55}$$

Calculating the $q\to 0$ limit of Eq. (54) and using the XC sum rule from Eq. (50) we obtain the following relation between φ and A:

$$\varphi=\left[-\frac{3}{32\sqrt{\pi}A}\right]^{2/3}\bar{\rho}^{-2/3},\quad A<0\ . \tag{56}$$

The dependence of φ and A on the density $\bar{\rho}$ could be obtained by calculating the XC energy density ε_{xc} of our model in the homogeneous limit yielding

$$\varepsilon_{xc}(\bar{\rho})=2\pi A\varphi\bar{\rho}\ . \tag{57}$$

For example, taking A to be independent on $\bar{\rho}$ leads to $\varepsilon_{xc}(\bar{\rho})\sim\bar{\rho}^{1/3}$. We should like to remark that also in the Green's-function approach, $\rho^{1/3}$-dependent models for the self-energy of insulating systems have been derived.[38,39] The final expression for v_{xc} from Eq. (47) with f_{xc} according to Eq. (52) reads

$$v_{xc}(q)=-\left[f_{xc}(q)-\frac{A}{9}\varphi q^2(7+2\varphi q^2)v(q)e^{-\varphi q^2}\right]\ . \tag{58}$$

Here we have taken A to be independent of $\bar{\rho}$ as a simplifying assumption. If found necessary the $\bar{\rho}$ dependence of A could be introduced with the help of Eqs. (47)–(49) and (52). In the small-q limit the local-field factor $G(q)$ as derived from Eq. (58) shows the correct q^2 behavior[31] and a $\bar{\rho}$ dependence could also be obtained from the long-wavelength limit of $G(q)$ which is related to the compressibility of an interacting-electron gas.[40]

IV. APPLICATIONS AND DISCUSSION

In this section we shall apply the theory for the band-structure potential developed in Sec. II and the model for exchange correlation of Sec. III to Si as an example for a prototype semiconductor.

In order to get an impression how the XC hole looks like we calculate the function $\bar{f}_{xc}(|\mathbf{r}-\mathbf{r}'|)\rho(\mathbf{r}')$ which corresponds to $\rho_{xc}(\mathbf{r},\mathbf{r}')$ in our model. Following the discussion in Sec. III we find for A and φ in Si the values $A=-0.798$ and $\varphi=0.0162a^2$ (a, lattice constant). In Fig. 2, $\bar{f}_{xc}(r)$ is plotted. According to its definition $\bar{f}_{xc}$ determines the range of the XC hole.

The size of the hole depends on the parameters φ, A, and $\bar{\rho}$ which are linked together by the XC sum rule from Eq. (56). A is related to the pair correlation function via Eq. (49). As can be seen from Fig. 2 for Si the values of φ, A, and $\bar{\rho}$ lead to a relatively tight XC hole. Figures 3(a) and 3(b) display the results for the XC hole in our model. Two different locations $\mathbf{r}$ for the electron have been tested. In Fig. 3(a) the electron is located at the bonding site while in Fig. 3(b) it is at the antibonding site. The results are similar to those given in Refs. 32 and 41, where the weighted-density approximation (WDA), i.e., a more involved procedure has been used. From its construction the density prefactor $\rho(\mathbf{r}')$ has the proper argument, $\mathbf{r}'$. This is not the case in the local-density approximation where $\rho(\mathbf{r})$ is used, i.e., the density prefactor is changed to the local point $\mathbf{r}$. However, physically the suppression of the probability of finding an electron at $\mathbf{r}'$, if another one is at $\mathbf{r}$, should be proportional to $\rho(\mathbf{r}')$. From Figs. 3(a) and 3(b) we extract further that the XC hole is anisotropic according to the actual charge density. This is in contrast to LDA where the hole is spherically symmetric and always centered on the electron at $\mathbf{r}$. Figure 3(b) explicitly demonstrates that this is not the case in our model. In accordance with the WDA results the hole is shifted away from the electron at $\mathbf{r}$ toward the bond. As a result nonlocality seems to be quite well reproduced by our homogeneous model for f_{xc}. Figure 4 displays $v_{xc}(q)$ from Eq. (58) for Si together with the related functions $v(q)$, $\bar{v}(q)$, and $-f_{xc}(q)$. The limiting values of v_{xc} are

$$\lim_{q\to 0}v_{xc}(q)=-\frac{8\pi}{9}A\varphi,\quad v_{xc}(q)\sim\frac{4\pi[1-g(0)]}{q^2}\quad \text{as } q\to\infty\ . \tag{59}$$

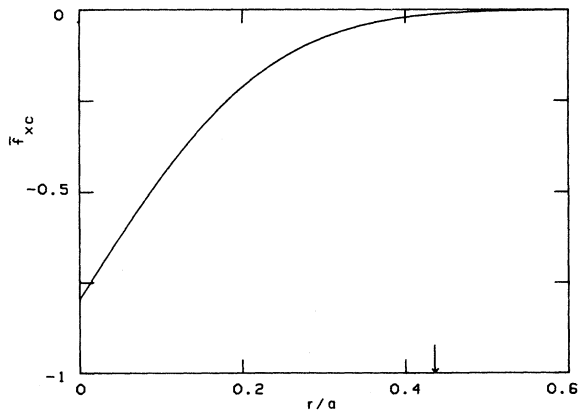

FIG. 2. Plot of the function $\bar{f}_{xc}(r)$ according to Eq. (51) which determines the extent of the XC hole in the model, a being the lattice constant. The nearest-neighbor distance is marked by an arrow.

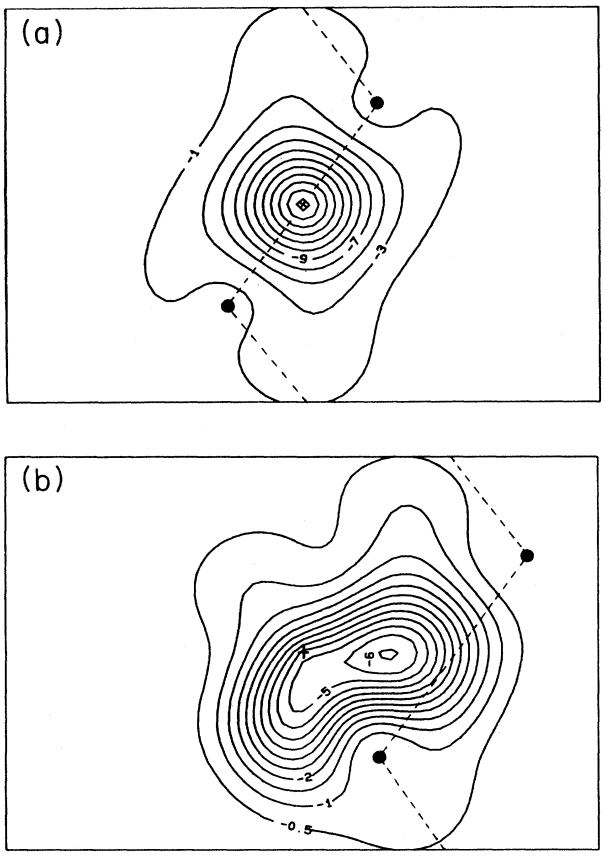

FIG. 3. Contour plots of the XC hole in Si in the $(0,-1,1)$ plane: (a) the electron is located at the bonding site, (b) the electron is located at the antibonding site. Units are electrons per cell.

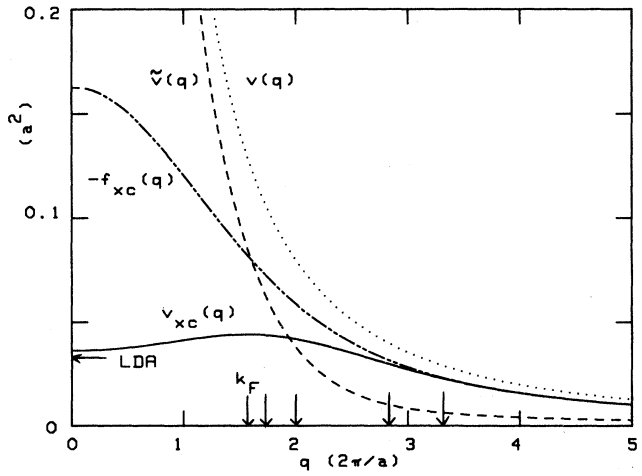

FIG. 4. Plot of the Fourier-transformed exchange-correlation interaction $v_{xc}(q)$ for Si from Eq. (58). Further, the functions $v(q)$, $\tilde{v}(q)$, and $-f_{xc}(q)$ defined in the text are drawn, a being lattice constant. The Fermi wave vector k_F and the first four reciprocal-lattice vectors are marked by arrows. The value of v_{xc} in the homogeneous limit of LDA is indicated.

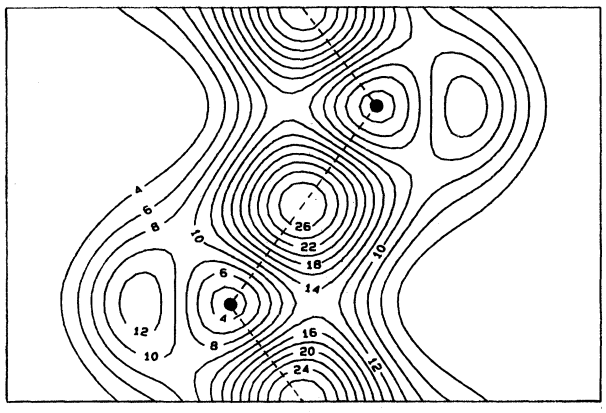

FIG. 5. Contour plot of the total valence charge density $\rho(\mathbf{r})$ of Si in the $(0,-1,1)$ plane as obtained by superposition of the partial densities (Fig. 1). Units as in Fig. 1.

Such a behavior should be contrasted with the homogeneous-limit form of LDA. Here v_{xc} is independent of $\mathbf{q}$ because of the local-density approximation.[42,43] In particular the diagonal part of v_{xc} is constant and indicated in Fig. 4.

We have reproduced in Fig. 5 the total valence charge density $\rho(\mathbf{r})$ of Si in the $(0,-1,1)$ plane determined as a superposition of the model partial densities from Fig. 1. Figure 6 shows the corresponding phonon dispersion of Si in the $\Delta(1,0,0)$ direction as obtained from the quasi-

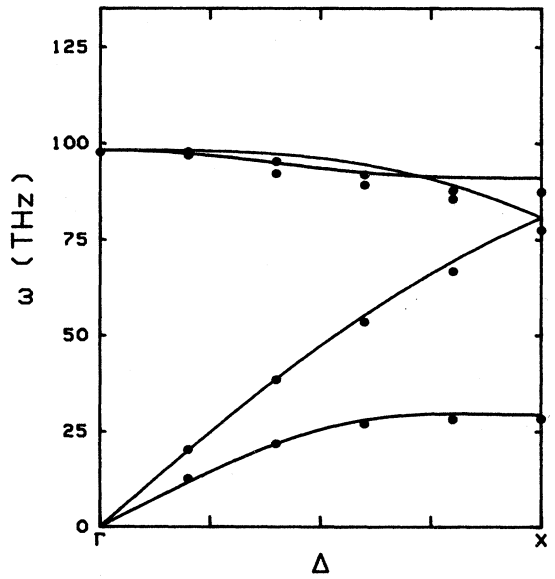

FIG. 6. Phonon dispersion curves for Si in the $\Delta(1,0,0)$ direction as calculated from the model partial density and the pseudopotential in Eq. (60). In addition to the rigid shift of ρ_α, rotations of the first- and second-nearest-neighbor quasi-ions have been taken into account. The dots indicate the experimental data.

ion approach with the model density ρ_α from Fig. 1. For the bare ions we have used an Appelbaum-Hamann–type potential

$$V_\alpha(q) = -\frac{4\pi Z_\alpha}{q^2}(1 - Aq^2 - Bq^4)e^{-Cq^2}, \tag{60}$$

with $A = -0.729\,86 \times 10^{-3} a^2$, $B = 0.203\,13 \times 10^{-4} a^4$, and $C = 0.389\,01 \times 10^{-2} a^2$. The phonon frequencies have been calculated by taking into account first- and second-neighbor rotations of the quasi-ions, see Refs. 21 and 26 for details. Using these expressions for V_α and ρ_α together with v_{xc} from Eq. (58) we are able to calculate the quasi-ion potentials $\tilde{V}_\alpha$ and the crystal potential $\tilde{V}$ according to Eqs. (23)–(27) or Eqs. (12) and (28), respectively. The result for the quasi-ion potential $\tilde{V}_\alpha(\mathbf{r})$ and the corresponding crystal potential $V_{\text{eff}}(\mathbf{r})$ obtained by superposition is presented in Figs. 7(a) and 7(b). The distribution of $\tilde{V}_\alpha(\mathbf{r})$ is spherical around the atomic sites quite in contrast to the corresponding partial density from Fig. 1 from which the quasi-ion potential is constructed. This behavior has its origin in the contribution of the bare pseudopotential and the "weighting factor" $\bar{v}$ in front of ρ_α in Eqs. (24) and (26) by which the nonspherical contributions of ρ_α related mainly to the large Fourier components are suppressed (Fig. 4). Further, we observe an attractive ring-shaped minimum of the quasi-ion potential at about the same distance from the ion where the

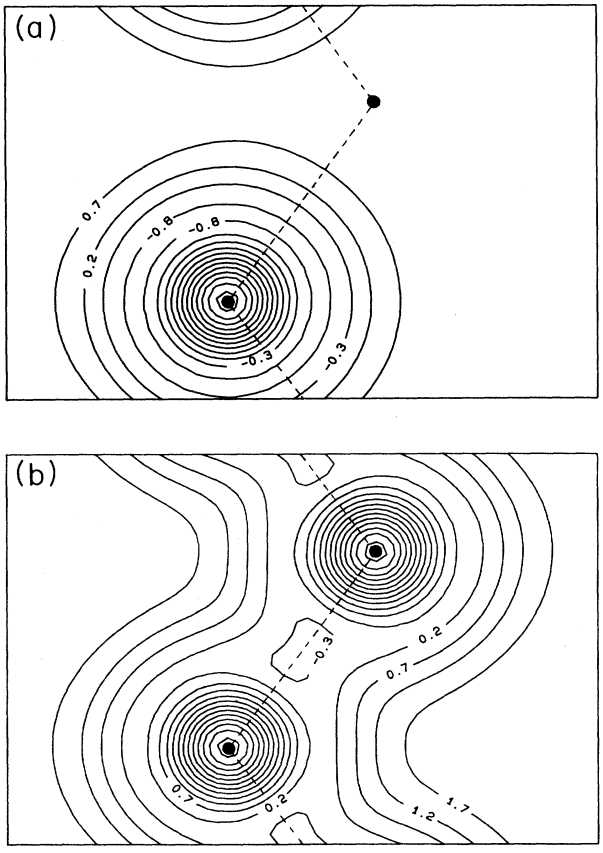

FIG. 7. Contour plot of the quasi-ion potential $\tilde{V}_\alpha(\mathbf{r})$ (a) and the total crystal potential $V_{\text{eff}}(\mathbf{r})$ of Si in the $(0,-1,1)$ plane (b). Units are in $4/a$.

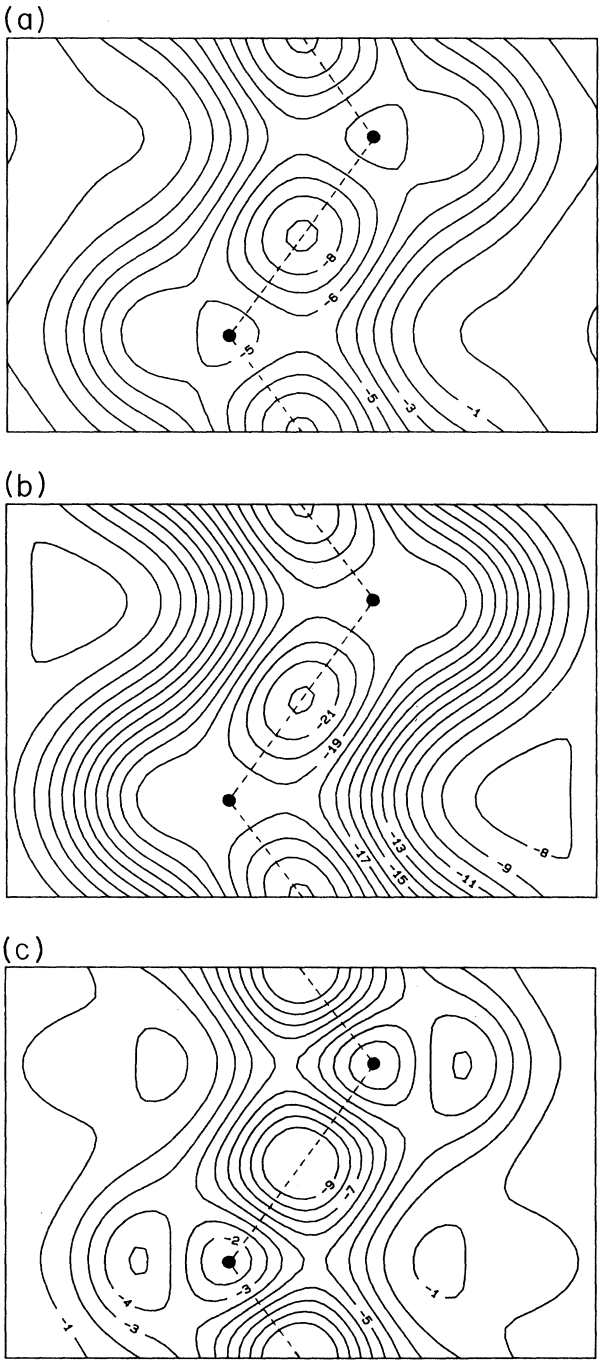

FIG. 8. Contour plots in the $(0,-1,1)$ plane of the exchange-correlation potential $V_{xc}(\mathbf{r})$ for the calculations discussed in the text. (a) is the result of V_{xc} in case the full expression for v_{xc} from Eq. (58) is used. (b) results if v_{xc} is approximated by $-f_{xc}$. (c) corresponds to the local approximation $v_{xc}(q \to 0)$. Units for V_{xc} are in eV.

TABLE I. Comparison of the calculated band energies at high-symmetry points to experimental data for Si. The different theoretical models for v_{xc} are discussed in the text. The data assigned to V_{xc} (LDA) and $V_{xc}(q\to 0)$ have been obtained self-consistently within the usual local-density-functional theory (LDF) (Ref. 15) using the ionic potential from Eq. (60). V_{xc} (LDA) is based on the Ceperley-Alder interpolation. $V_{xc}(q\to 0)$ is derived analogously to $v_{xc}(q)$ applying only the first functional derivative to E_{xc} from Eq. (44). The result corresponds to an $X\alpha$-type approximation with $\alpha=0.74$.

	v_{xc}(LDA)	$v_{xc}(q\to 0)$	v_{xc}	$-f_{xc}$	$v_{xc}=0$	Expt.	V_{xc}(LDA)	$V_{xc}(q\to 0)$
E_g	0.91	1.19	1.12	2.37	−1.37	1.17	0.99	1.05
$\Gamma'_{25v}\to\Gamma_{15c}$	3.23	3.44	3.21	3.97	1.47	3.4	3.03	3.07
$\Gamma_{1v}\to\Gamma'_{25v}$	12.52	12.40	12.57	12.27	13.54	12.5±0.6	12.75	12.73
$\Gamma'_{25v}\to\Gamma'_{2c}$	4.21	4.35	3.77	3.57	3.08	4.2	3.52	3.55
$\Gamma_{15c}\to\Gamma'_{2c}$	0.98	0.91	0.56	−0.40	1.61	0.8	0.49	0.48
$X_{4v}\to\Gamma'_{25v}$	3.01	2.91	2.99	2.61	3.94	2.9, 3.3±0.2	3.06	3.05
$\Gamma'_{25v}\to X_{1c}$	1.05	1.33	1.28	2.57	−1.35	1.3	1.17	1.23
$L'_{2v}\to\Gamma'_{25v}$	10.13	10.05	10.24	10.13	10.79	9.3±0.4	10.44	10.43
$L_{1v}\to\Gamma'_{25v}$	7.28	7.14	7.26	6.82	8.62	6.7±0.2	7.43	7.40
$L'_{3v}\to\Gamma'_{25v}$	1.26	1.22	1.28	1.14	1.64	1.2±0.2, 1.5	1.31	1.29
$\Gamma'_{25v}\to L_{1c}$	2.03	2.22	1.97	2.56	0.62	2.1, 2.4±0.15	1.79	1.83
$\Gamma'_{25v}\to L_{3c}$	4.00	4.24	4.08	5.06	1.88	4.15±0.1	3.93	3.98
$L'_{3v}\to L_{1c}$	3.29	3.44	3.25	3.70	2.26	3.45	3.10	3.12
$L'_{3v}\to L_{3c}$	5.26	5.46	5.36	6.20	3.52	5.50	5.24	5.27

partial density reaches its maximum. In this way the electrons are attracted very efficiently into that space region. The total band-structure potential $V_{eff}(\mathbf{r})$ from Fig. 7(b) displays a spherical (repulsive) shape around the ions and an attractive minimum region at the bond center. Here the charge density has its maximum. This minimum region of the potential is elongated along the bonding chain and results from the superposition of the ring-shaped minima of the quasi-ion potentials $\tilde{V}_\alpha(\mathbf{r})$. In the empty-space region of the structure the potential is repulsive. Thus the charge is strongly pushed away and becomes condensed along the chains.

In Fig. 8(a) the exchange-correlation potential $V_{xc}(\mathbf{r})$ for Si as obtained from Eqs. (23)–(27) and Eq. (58) is shown as a contour plot in the $(0,-1,1)$ plane. It is most attractive at the bond center, which is important for the direct band gap because the (Γ'_{25v}) density of the wave function at the valence-band maximum (bonding p type in an atomic orbital picture) is mainly localized in that region. Thus the attraction of V_{xc} at the bond center is a measure for the decrease in energy of the Γ'_{25v} state. On the other hand, the (Γ_{15c}) density of the lowest-conduction-band wave function at point Γ (antibonding p type) has maxima around the antibonding sites. In this region of space V_{xc} is less attractive, leading finally to a band gap. Qualitatively, the size of the band gap should be determined in first order by the difference of $V_{xc}(\mathbf{r})$ at the bonding site and the antibonding site, respectively. This can be confirmed by inspection of Table I and by examination of the corresponding values of V_{xc} in Figs. 8(a)–8(c), where different models have been investigated.

Figure 9 shows the calculations of the theoretical band structure of Si (solid curves) as obtained within the quasi-ion approach using Eq. (58) for the exchange-correlation interaction. The results are compared with the empirical band structure (dashed curves) along the main symmetry directions Δ, Σ, and Λ. Good agreement of both calculations can be observed. Furthermore, the conformity with the experimental data can be extracted from Table I, where the calculated band energies are compared to experiment[14] at high-symmetry points.

The detailed shape of $V_{xc}(\mathbf{r})$ is determined by the degree of nonlocality introduced by $v_{xc}(\mathbf{r}-\mathbf{r}')$ "acting" on the density $\rho(\mathbf{r}')$; compare Figs. 8(a)–8(c) and Fig. 10. This can be seen by integration of Eq. (36) taking for v_{xc} the approximate form $v_{xc}(\mathbf{r}-\mathbf{r}')$

$$V_{xc}(\mathbf{r})=-\int dV' v_{xc}(\mathbf{r}-\mathbf{r}')\rho(\mathbf{r}') \ . \tag{61}$$

The solid curve in Fig. 10 represents $v_{xc}(|\mathbf{r}|)$ from our

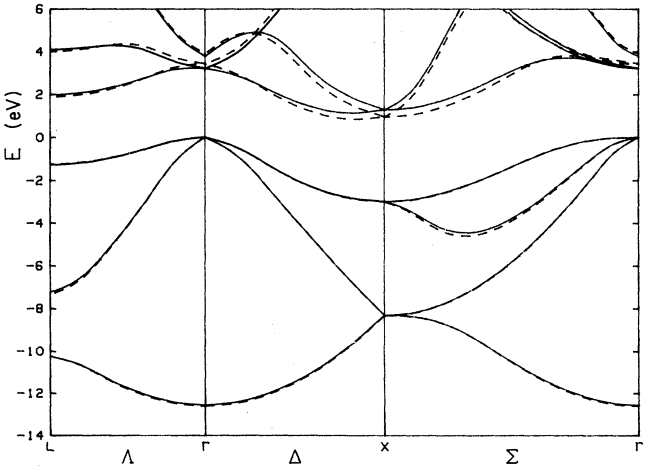

FIG. 9. Comparison of the theoretical band structure of Si (solid curves) in the main symmetry directions Δ, Σ, and Λ with the corresponding empirical results from Cohen and Bergstresser (dashed curves). Energies are in eV. The valence-band maximum is normalized to zero.

model which is translationally as well as rotationally invariant.[21] We find a relatively short-ranged behavior for the nonlocality in v_{xc}. It is of the order of half a bond length in Si. Comparing v_{xc} with the approximate expression $-f_{xc}$ which results from v_{xc} if the derivatives of f_{xc} with respect to the density $\bar{\rho}$ are ignored in Eq. (47), we find that v_{xc} is considerably tighter. This can also be seen qualitatively from the Fourier-transformed quantities represented in Fig. 4. From this plot it might be expected that even a local approximation for v_{xc} could be reasonable because $v_{xc}(q)$ is roughly a constant for the most important small reciprocal-lattice vectors. This supposition is strengthened by calculating the function $v_{xc}(\mathbf{r}-\mathbf{r}')\rho(\mathbf{r}')$ itself. The results are displayed in Figs. 11(a)–11(c) in the $(0,-1,1)$ plane for three different positions of $\mathbf{r}$ (bonding site, antibonding site, and interstitial site). The most important feature of $-v_{xc}\rho$ is a strongly localized 'hole" (with different amplitude) which is approximately spherical and centered at $\mathbf{r}=\mathbf{r}'$.

In order to test the influence of the detailed shape of $V_{xc}(\mathbf{r})$ on the band structure we have investigated two additional models approximating v_{xc} by $-f_{xc}$, Fig. 8(b), and by its value in the long-wavelength limit, i.e., $v_{xc}(q\rightarrow 0)$, Fig. 8(c). This leads to qualitatively different results for $V_{xc}(\mathbf{r})$. We would like to mention that a local approximation for v_{xc} like the value of v_{xc} for $q\rightarrow 0$ or the LDA value in the homogeneous limit indicated in Fig. 4 yield for $V_{xc}(\mathbf{r})$ a contour line plot [Fig. 8(c)] which can be obtained from Fig. 5 by scaling the density with the corresponding constant of Fig. 4 at $q=0$.

In accordance with the deeper values of $V_{xc}(\mathbf{r})$ along the bonding chain (and in the antibonding region, see above) we get in case of $-f_{xc}$ both a lower valence-band maximum and a lower conduction-band minimum at Γ, see Fig. 12(a). However, the energy of the top of the valence band (in fact the whole valence-band complex) is more decreased than the conduction band. This leads to a larger direct band gap and indirect band gap as compared with the model based on the complete expression for v_{xc}; notice also the definite energy values listed in Table I.

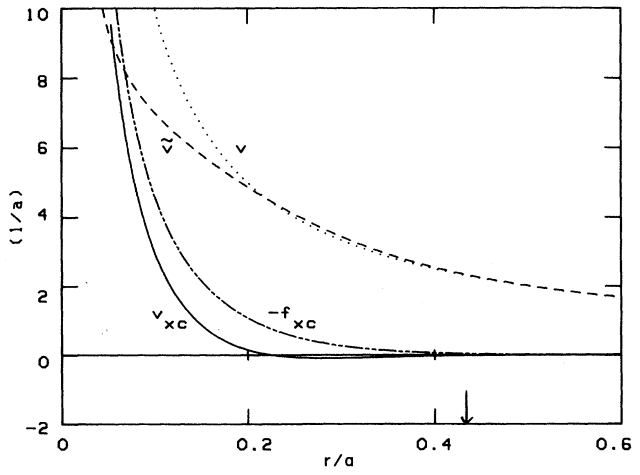

FIG. 10. Plot of the exchange-correlation interaction $v_{xc}(r)$ and the functions $-f_{xc}(r)$, $\tilde{v}(r)$, and $1/r$. The nearest-neighbor distance is marked by an arrow.

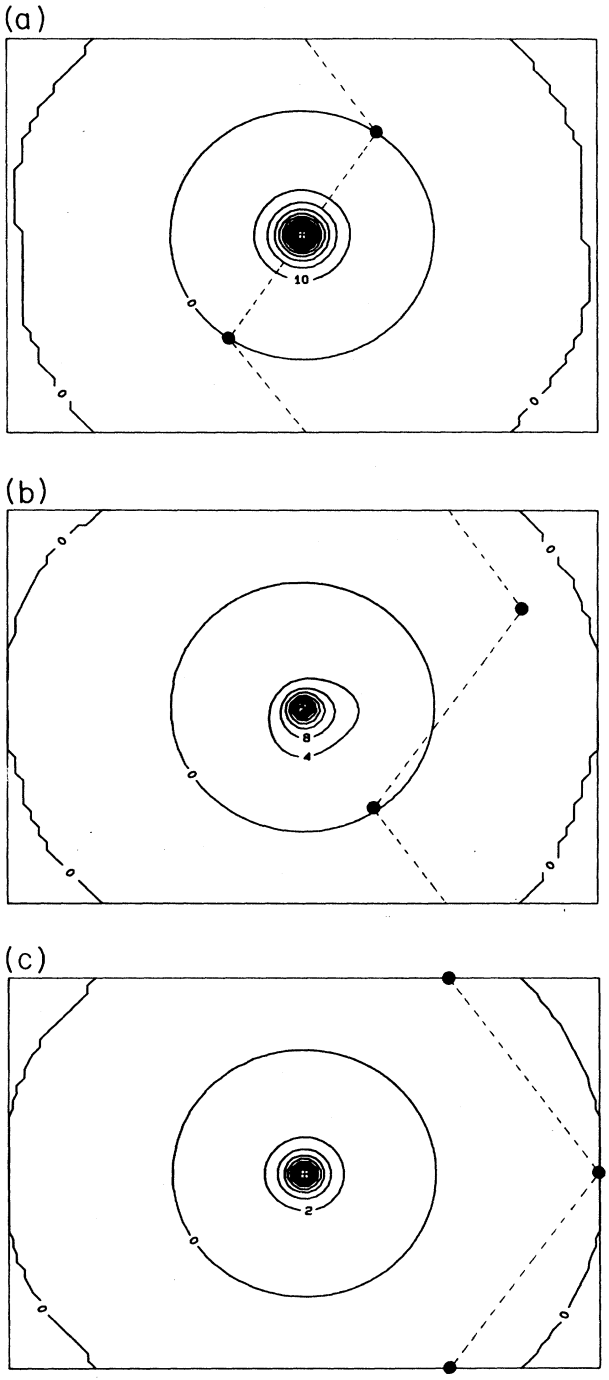

FIG. 11. Contourline plots of $v_{xc}(\mathbf{r}-\mathbf{r}')\cdot\rho(\mathbf{r}')$ for three different positions of $\mathbf{r}$: (a) bonding site, (b) antibonding site, and (c) interstitial site. Units are in $40/a^4$, a being the lattice constant. Compare with Fig. 3.

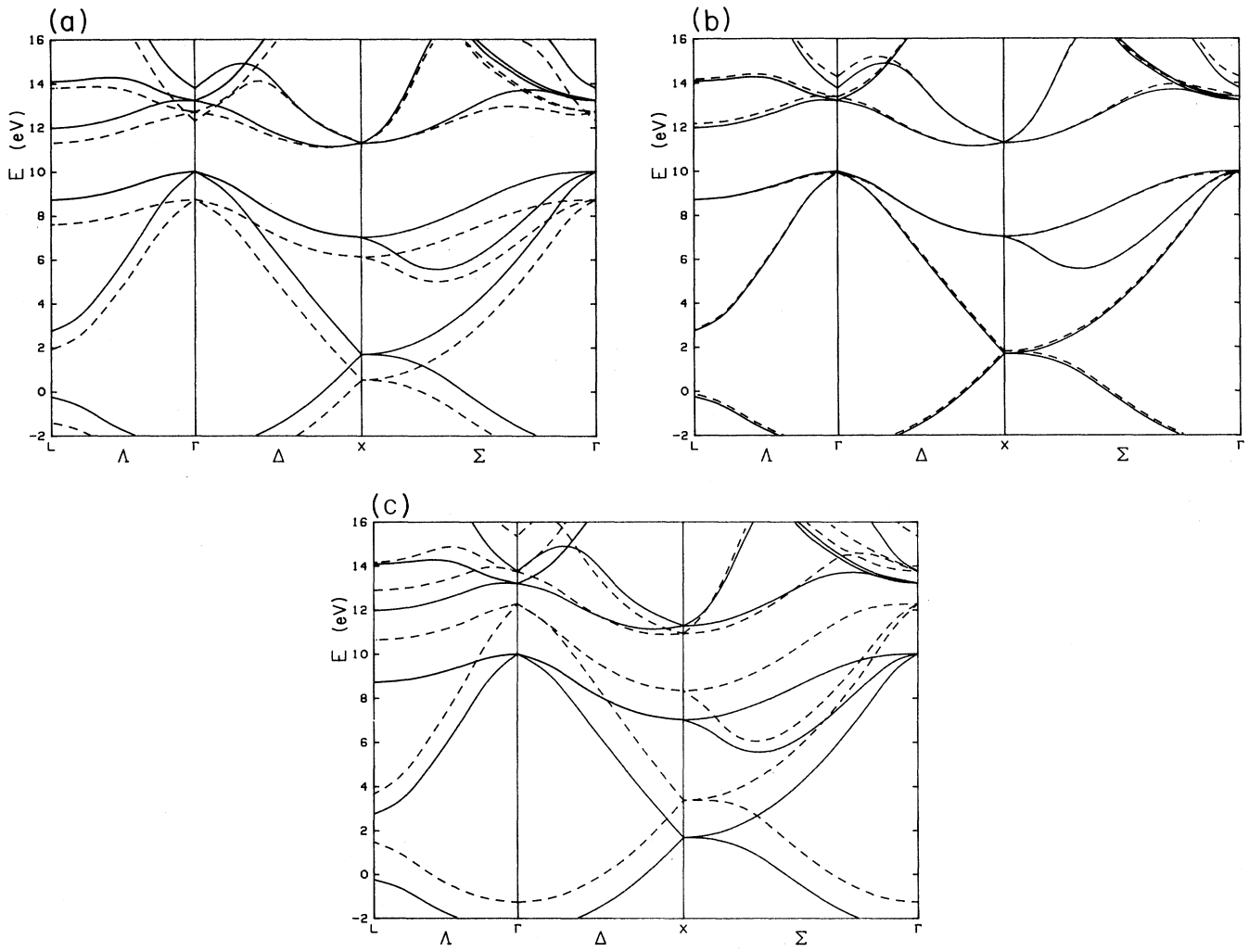

FIG. 12. Comparison of different theoretical band structures of Si in the main symmetry directions. In these calculations the band structures for the different models have been shifted by the corresponding constants $\tilde{V}(0)$ in order to compare the relative values of the energies. Several approximations for the exchange-correlation interaction are compared: (a) v_{xc} (solid curves), $-f_{xc}$ (dashed curves); (b) v_{xc} (solid curves), $v_{xc}(q\rightarrow 0)$ (dashed curves); (c) v_{xc} (solid curves), $v_{xc}=0$ (dashed curves).

The Γ_{15c} density is minimal parallel to the bonding chains and assumes its maxima near the antibonding sites. On the other hand, the Γ'_{2c} density has its minimum region around the bond center extending into the space transverse to the bond and its maxima around the atoms halfway to the antibonding sites. Thus, for the relative ordering of Γ_{15c} and Γ'_{2c} in the energy spectrum the detailed shape of $V_{xc}(\mathbf{r})$ around the atoms, the bonding and the antibonding region is crucial. This is illustrated best by comparing V_{xc} as represented in Figs. 8(b) and 8(c). In these models the exchange-correlation potentials are qualitatively different. In Fig. 8(b), V_{xc} is elongated parallel to the bond and displays a large increase in the antibonding region. On the other hand, V_{xc} from Fig. 8(c) is spherical to slightly elongated transverse to the bond and nearly flat in the antibonding region. Such a behavior leads to an energy split between Γ'_{2c} and Γ_{15c} of approximately the correct size, see Table I, while in the first case the energy levels even have changed their positions in the spectrum. In case of V_{xc} from Fig. 8(a) the difference in energy is smaller than for V_{xc} from Fig. 8(c). This is not unexpected because the shape of V_{xc} is intermediate between that of Figs. 8(b) and 8(c).

Figure 12(b) demonstrates good agreement of the local approximation with the nonlocal calculation, thus a local approximation seems to be justified within the quasi-ion formalism. The results for the band structure in the homogeneous limit of LDA [v_{xc} (LDA) in Table I] are in general comparable with those using $v_{xc}(q\rightarrow 0)$. The direct and indirect band gaps are a bit smaller in this calculation.

Finally, in order to see what happens if exchange-correlation contributions are ignored at all in $\tilde{v}$ we can take a look in Fig. 12(c). The dominant effect is a large

upward shift of the valence band leading to a very small direct band gap and to a negative indirect one. Furthermore, the width of the valence band is increased ($v_{xc}=0$ in Table I).

We conclude this discussion by noting that the quality of the band structure could certainly be improved further by using simultaneously a more extended basis set of expansion functions in Eq. (11) and by varying the parameters in the ion pseudopotential without destroying the quality of the phonon dispersion. In particular the Γ'_{2c} state could be improved by changing the pseudopotential because of its localization at the atoms.

We certainly are aware of the fact that even in the exact DFT we still have to deal with the low-band-gap problem. How large the difference between the true quasiparticle energy gap and the DFT band gap really is, is still a matter of controversy.[44,45] From our results we learn that a good band structure for Si can be calculated with use of the quasi-ion approach and the factorized form of the exchange-correlation potential. Because the crystal potential depends on the density itself, the calculations of the quasi-ion densities should be carried out self-consistently. Calculations along these lines will be performed in future work.

Note added in proof. We would like to remark that the gap will change with the value of the lattice constant used in the calculation. It can be expected to be smaller for a lattice constant which would result from a minimization of the total energy of Si using the Appelbaum-Hamann potential because such a procedure leads to a smaller lattice constant and consequently to a more metallic behavior with a smaller gap, independent of the model used for exchange-correlation effects.

ACKNOWLEDGMENTS

We would like to thank Dr. P. Krüger for useful discussions. Support by the Deutsche Forschungsgemeinschaft (Bonn, Germany), under Project No. Fa-170/1-3 is gratefully acknowledged.

[1]M. L. Cohen and T. K. Bergstresser, Phys. Rev. **141**, 789 (1966).
[2]J. P. Walter and M. L. Cohen, Phys. Rev. B **4**, 1877 (1971).
[3]J. R. Chelikowsky and M. L. Cohen, Phys. Rev. B **14**, 556 (1976).
[4]J. A. Appelbaum and D. R. Hamann, Phys. Rev. B **8**, 1777 (1973).
[5]M. Schlüter, J. R. Chelikowsky, S. G. Louie, and M. L. Cohen, Phys. Rev. B **12**, 4200 (1975).
[6]D. R. Hamann, Phys. Rev. Lett. **42**, 662 (1979).
[7]G. B. Bachelet and N. E. Christensen, Phys. Rev. B **31**, 879 (1985).
[8]P. Hohenberg and W. Kohn, Phys. Rev. **136**, B864 (1964).
[9]W. Kohn and L. J. Sham, Phys. Rev. **140**, A1133 (1965).
[10]J. P. Perdew and M. Levy, Phys. Rev. Lett. **51**, 1884 (1983).
[11]L. J. Sham and M. Schlüter, Phys. Rev. Lett. **51**, 1888 (1983); Phys. Rev. B **32**, 3883 (1985).
[12]L. Hedin and S. Lundqvist, in *Solid State Physics,* edited by H. Ehrenreich, F. Seitz, and D. Turnbull (Academic, New York, 1969), Vol. 23.
[13]C. Strinati, H. J. Mattausch, and W. Hanke, Phys. Rev. B **25**, 2867 (1982).
[14]M. S. Hybertsen and S. G. Louie, Phys. Rev. B **34**, 5390 (1986).
[15]P. Krüger (private communication).
[16]W. von der Linden and P. Horsch, Phys. Rev. B **37**, 8351 (1988).
[17]R. W. Godby, M. Schlüter, and L. J. Sham, Phys. Rev. B **37**, 10 159 (1988).
[18]C. Falter, M. Selmke, W. Ludwig, and K. Kunc, Phys. Rev. B **32**, 6518 (1985).
[19]C. Falter, W. Ludwig, A. A. Maradudin, M. Selmke, and W. Zierau, Phys. Rev. B **32**, 6510 (1985).
[20]C. Falter, W. Ludwig, M. Selmke, and W. E. Pickett, J. Phys. C **20**, 501 (1987).
[21]C. Falter, Phys. Rep. **164**, 1 (1988); **164**, 2 (1988).
[22]M. Born and R. Oppenheimer, Ann. Phys. (N.Y.) **84**, 457 (1927).
[23]G. D. Whitfield, Phys. Rev. **121**, 720 (1961).
[24]K. W. Stevens, J. Phys. C **6**, 2191 (1973).
[25]M. Wagner, Phys. Status Solidi B **107**, 617 (1981).
[26]C. Falter, H. Rakel, and W. Ludwig, Phys. Rev. B **38**, 3986 (1988).
[27]H. Rakel, C. Falter, and W. Ludwig, J. Phys. F **18**, 2181 (1988).
[28]K. S. Singwi and M. P. Tosi, in *Solid State Physics,* edited by H. Ehrenreich, F. Seitz, and D. Turnbull (Academic, New York, 1981), Vol. 36.
[29]W. E. Pickett, J. Phys. C **12**, 1491 (1979).
[30]O. Gunnarsson, M. Jonson, and B. I. Lundqvist, Phys. Rev. B **20**, 3136 (1979).
[31]K. Utsumi and S. Ichimaru, Phys. Rev. B **22**, 1522 (1980).
[32]M. S. Hybertsen and S. G. Louie, Phys. Rev. B **30**, 5777 (1984).
[33]J. C. Kimball, Phys. Rev. A **7**, 1648 (1973).
[34]H. Yasuhara, Solid State Commun. **11**, 1481 (1972).
[35]J. G. Zabolitzky, Phys. Rev. B **22**, 2353 (1980).
[36]D. Ceperley, Phys. Rev. B **18**, 3126 (1978).
[37]*Handbook of Mathematical Functions,* edited by M. Abramowitz and I. A. Stegun (Dover, New York, 1972).
[38]W. Hanke, Th. Gölzer, and H. J. Mattausch, Solid State Commun. **51**, 23 (1984).
[39]P. A. Sterne and J. C. Inkson, J. Phys. C **17**, 1497 (1984).
[40]L. Hedin and B. I. Lundqvist, J. Phys. C **4**, 2064 (1971).
[41]P. Krüger, G. Wolfgarten, and J. Pollmann, Solid State Commun. **53**, 885 (1985).
[42]In-Whan Lyo and E. W. Plummer, Phys. Rev. Lett. **60**, 1558 (1988).
[43]J. E. Northrup, M. S. Hybertsen, and S. G. Louie, Phys. Rev. Lett. **59**, 819 (1987).
[44]L. J. Sham and M. Schlüter, Phys. Rev. Lett. **60**, 1582 (1988).
[45]O. Gunnarsson and K. Schönhammer, Phys. Rev. Lett. **56**, 1968 (1986); **60**, 1583 (1988).